



## On the sensitivity of the Devonian climate to continental configuration, vegetation cover and insolation

Julia Brugger<sup>1,2,3</sup>, Matthias Hofmann<sup>1</sup>, Stefan Petri<sup>1</sup>, and Georg Feulner<sup>1</sup>

<sup>1</sup>Potsdam-Institut für Klimafolgenforschung (PIK), Mitglied der Leibniz-Gemeinschaft, Postfach 60 12 03, 14412 Potsdam, Germany

<sup>2</sup>Universität Potsdam, Institut für Physik und Astronomie, Karl-Liebknecht-Straße 24/25, 14476 Potsdam, Germany

<sup>3</sup>Berlin-Brandenburgisches Institut für Biodiversitätsforschung, Altensteinstraße 34, 14195 Berlin, Germany

*Correspondence to:* Julia Brugger ([brugger@pik-potsdam.de](mailto:brugger@pik-potsdam.de)) and Georg Feulner ([feulner@pik-potsdam.de](mailto:feulner@pik-potsdam.de))

**Abstract.** During the Devonian period (419 to 359 million years ago), life on Earth witnessed decisive evolutionary breakthroughs, most prominently the colonisation of land by vascular plants and vertebrates. At the same time, it is also a period of major marine extinction events coinciding with marked changes in climate. There is limited knowledge about the causes of these changes and their interactions. It is therefore instructive to explore systematically how the Devonian climate system responds to changes in critical boundary conditions. Here we use coupled climate-model simulations to investigate separately the influence of changes in orbital parameters, continental configuration and vegetation cover on the Devonian climate. Variations of Earth's orbital parameters affect the Devonian climate system, with the warmest climate states at high obliquity and high eccentricity, but the amplitude of global temperature differences is smaller than suggested by an earlier study based on an uncoupled atmosphere model. The prevailing mode of climate variability on decadal to centennial timescales relates to surface air temperature fluctuations in high northern latitudes which are mediated by coupled oscillations involving sea-ice cover, ocean convection and a regional overturning circulation in the Arctic. Furthermore, we find only a small biogeophysical effect of changes in vegetation cover on global climate during the Devonian, and the impact of changes in continental configuration is small as well. Assuming decreasing atmospheric carbon dioxide concentrations throughout the Devonian, we then set up model runs representing the Early, Middle and Late Devonian. Comparing the simulations for these timeslices, the temperature evolution is dominated by the strong decrease in atmospheric carbon dioxide. In particular, the albedo change due to the increase in land vegetation alone cannot explain the temperature rise found in Late Devonian proxy data which remains difficult to reconcile with reconstructed falling carbon-dioxide levels. Simulated temperatures are significantly lower than estimates based on oxygen-isotope ratios, suggesting a lower  $\delta^{18}\text{O}$  ratio of Devonian seawater.

*Copyright statement.*



## 1 Introduction

The Devonian (419 to 359Ma, 1 Ma = 1 million years ago) is a key period in Earth's history characterised by fundamental changes in the atmosphere, the ocean and the biosphere. With respect to the evolution of life, it is best known for the diversification of fish as well as the colonisation of the continents by vascular plants and vertebrates. Although microbial mats and nonvascular plants could be found on land even before the Devonian (Boyce and Lee, 2017), the appearance of vascular land plants beginning in the Early and Middle Devonian was certainly an important first step towards modern land ecosystems. By the Late Devonian, vascular plants had vastly diversified, going hand in hand with the evolution of more advanced leaves and root systems (Algeo et al., 1995; Algeo and Scheckler, 1998). In the ocean, coral stromatoporoid reefs reached their largest extent during the Phanerozoic in the Middle Devonian (Copper and Scotese, 2003) and fish evolved into rich diversity (Dahl et al., 2010). Finally, in the Late Devonian, the first tetrapods moved from ocean to land (Clack, 2007; Brezinski et al., 2009).

While the Devonian is best known for these evolutionary breakthroughs, it is also a period of species mass extinctions. The extinction rate during the Devonian is marked by three distinct peaks (Bambach, 2006), with the highest pulse ranking among the five most severe mass extinctions in Earth's history (Frasnian-Famennian mass extinction, 378–375Ma, Bambach 2006). The cause of these extinctions, which mostly took place in the ocean (Bambach, 2006), is still under debate, as it is challenging to explain the episodic nature and duration of the extinctions (Algeo et al., 1995). Discussed causes for the Frasnian-Famennian extinction are a bolide impact (McGhee et al., 1984), volcanic activity (Ma et al., 2016), changes in sea level (Bond and Wignall, 2008; Ma et al., 2016), rapid temperature variations (Ma et al., 2016) and the development of ocean anoxic waters (Bond and Wignall, 2008; Ma et al., 2016).

The multitude of remarkable biospheric changes during the Devonian occurred against a backdrop of considerable changes in atmospheric composition. In particular, carbon dioxide (CO<sub>2</sub>) concentrations decreased strongly from ~2,000 ppm to ~1,000 ppm (Foster et al., 2017) as shown in Fig. 1a. Note that this recent CO<sub>2</sub> compilation agrees with older compilations in the general decreasing trend during this time, but reports lower CO<sub>2</sub> concentrations for the Devonian than older proxy studies (Royer, 2006); they are also much lower than the CO<sub>2</sub> concentrations based on the GEOCARB model (Berner, 1994, 2006) frequently used in earlier modeling studies. In contrast to the decrease in carbon dioxide, oxygen levels witnessed an exceptionally strong rise about 400Ma (Dahl et al., 2010).

These changes in atmospheric composition, and in particular the drop in atmospheric CO<sub>2</sub> concentrations, also resulted in climatic changes, which in turn affected the biosphere. Indeed,  $\delta^{18}\text{O}$  oxygen isotope data (shown in Fig. 1b) indicate a greenhouse climate in the Early Devonian and much cooler temperatures in the Middle Devonian (Joachimski et al., 2009). For the Late Devonian, proxy studies (van Geldern et al., 2006; Joachimski et al., 2009) indicate rising temperatures again which are still challenging to reconcile with the decreasing CO<sub>2</sub> concentrations. During the late Famennian, Earth's climate cooled again (Brezinski et al., 2009; Joachimski et al., 2009), with some studies even indicating glaciations (Caputo, 1985; Caputo et al., 2008; Brezinski et al., 2008, 2009). Whether this is accompanied by a sea-level transgression linked to the development of ocean anoxic conditions (Johnson et al., 1985; Bond and Wignall, 2008) or a sea-level drop (Sandberg et al., 2002; Haq

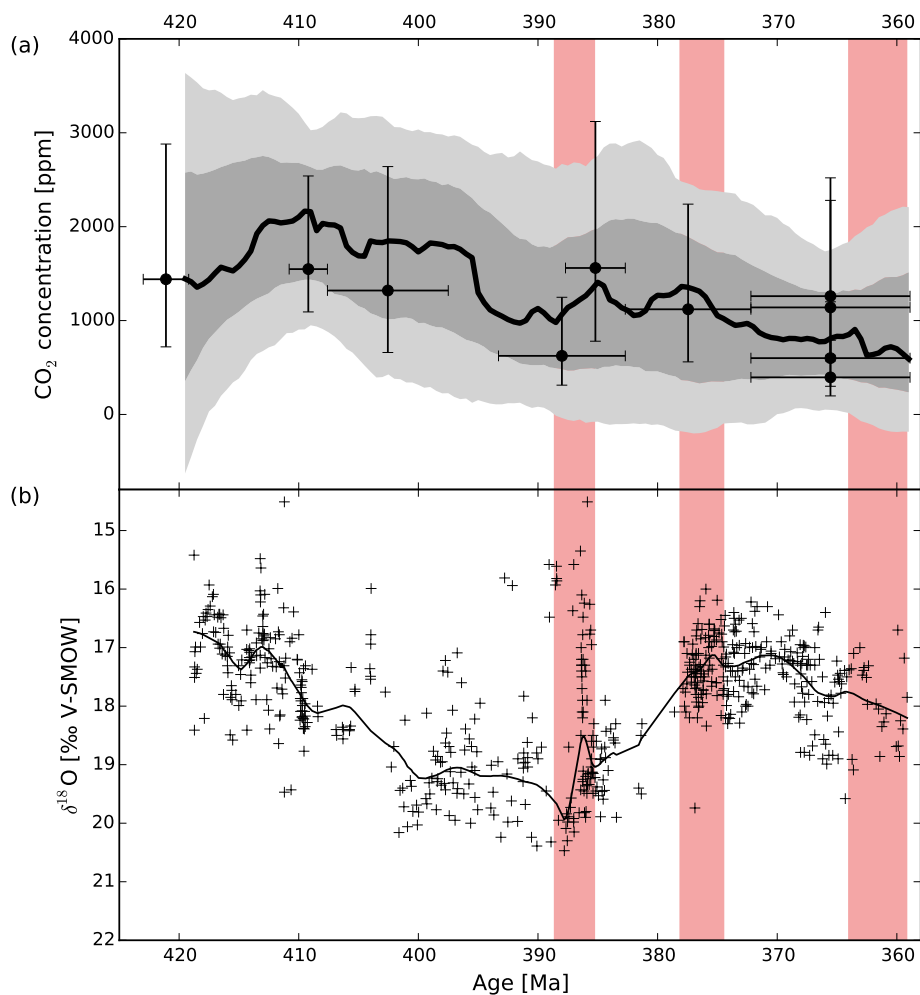


**Figure 1.** (a) Atmospheric CO<sub>2</sub> concentration in the Devonian after Foster et al. (2017). The black circles represent the data from different proxies. The thick black line is the most likely LOESS fit taking into account the uncertainties in both age and CO<sub>2</sub>. The dark and light grey bands show the 68% and 95% confidence intervals. (b)  $\delta^{18}\text{O}$  values from conodont apatite from Joachimski et al. (2009), but using a different NBS120c standard for calibration (Lécuyer et al., 2003). Note the inverted scale on the  $y$  axis since an increase in  $\delta^{18}\text{O}$  translates in a temperature decrease. The light pink shading indicates the time intervals of the three Devonian periods of mass extinction: the late Givetian extinction from 389 to 385 Ma, the Frasnian-Famennian extinction (or Kellwasser event) from 378 to 375 Ma, and the Late Famennian extinction (Hangenberg event) from 364 to 359 Ma (Bambach, 2006).

and Schutter, 2008; Ma et al., 2016) is still debated, but there is consent that the Late Devonian was a period of fast sea-level variations (Johnson et al., 1985; Sandberg et al., 2002; Haq and Schutter, 2008; Brezinski et al., 2009; Ma et al., 2016).



As any other period in Earth's history, the 60 million years spanning the Devonian are not only characterised by long-term changes in temperature, but also by large fluctuations in temperature around these longer-term trends (see Fig. 1b). Furthermore, there are several studies stressing the importance of astronomical forcing for the climate during the Devonian. The geologic record of the Devonian shows cyclic structures (De Vleeschouwer et al., 2013, 2017) which can be interpreted as the result of astronomical cycles according to Milankovitch theory (Milankovitch, 1941). The configuration of Earth's orbit and rotational axis determines the total amount as well as the spatial and temporal distribution of solar radiation, and therefore impacts climate. In addition, identifying astronomical cycles in the geologic record can help assigning a timescale to cyclic features observed in the geologic record, and thus a timescale for palaeoclimatic changes (De Vleeschouwer et al., 2013, 2014, 2017).

In an effort to link the changes in the various components of the Devonian Earth system, there are several studies investigating potential connections between land plant evolution, climate change and the oceanic mass extinction (Berner, 1994; Algeo et al., 1995; Algeo and Scheckler, 1998; Godderis and Joachimski, 2004; Simon et al., 2007; Le Hir et al., 2011). It is suggested, for example, that the increase of weathering due to the spreading of plants on land could have been a cause of the decrease in carbon dioxide (Algeo et al., 1995; Algeo and Scheckler, 1998; Berner, 2006). Additionally, the increased weathering rates could have lead to a higher transport of phosphorus to the ocean, promoting eutrophication with its negative consequences for life in the ocean (Algeo et al., 1995; Algeo and Scheckler, 1998).

Given the multitude of changes in the Earth system during the Devonian and the intricate coupling of atmosphere, ocean and biosphere, it is challenging to disentangle causes and effects and to determine which forcings are most important for Devonian climate change. In this study, we test the sensitivity of the Devonian climate to different forcings in order to quantify their relevance. We therefore set up simulations with a coupled ocean–atmosphere model considering three different continental configurations representing the Early, Middle and Late Devonian. In addition, changes in the solar constant, in atmospheric carbon dioxide concentrations, in orbital parameters and in the spatial distribution of vegetation are systematically tested. Concerning the influence of land plants, this study focuses on their impact on the climate via biogeophysical effects, in particular changes in albedo and evapotranspiration.

This paper is organised as follows. Section 2 describes the coupled climate model used in this study, the boundary conditions for the Devonian as well as the various sensitivity experiments. Results from these simulations are presented and discussed in Section 3, including an ocean–sea-ice mechanism resulting in climate oscillations at high northern latitudes and “best-guess” simulations for climate states which could be considered typical for the Early, Middle and Late Devonian, respectively, in terms of their continental configuration, vegetation cover, solar constant and carbon-dioxide concentration. Finally, Section 4 summarises our key findings and briefly discusses the broader implications of our results.

## 2 Modeling set-up

### 2.1 Model description

To be able to assess the sensitivity of the Devonian climate to a wide range of parameters, we use a relatively fast coupled Earth-system model of intermediate complexity (Montoya et al., 2005). Its main component consists of a modified version of



Sensitivity experiments	Continents	$S$ [ $\text{Wm}^{-2}$ ]	$\text{CO}_2$ [ppm]	Land cover	$\varepsilon$ [ $^\circ$ ]	$e$	$\omega$ [ $^\circ$ ]
Continental configuration	415 Ma						
	380 Ma	1319.1	1500	bare	23.5	0	0
	360 Ma						
Vegetation distribution				bare			
	360 Ma	1319.1	1500	coastal shrub trees	23.5	0	0
					22.0	0	0
Orbital parameters					22.0	0.030	0, 45, 90, 135, 180, 225, 270, 315
					22.0	0.069	0, 45, 90, 135, 180, 225, 270, 315
					23.5	0	0
	380 Ma	1319.1	1500	bare	23.5	0.030	0, 45, 90, 135, 180, 225, 270, 315
					23.5	0.069	0, 45, 90, 135, 180, 225, 270, 315
					24.5	0	0
Best-guess simulations	415 Ma	1315.3	2000	bare			
	380 Ma	1319.1	1500	coastal shrub	23.5	0	0
	360 Ma	1321.3	1000	trees			

**Table 1.** Overview of simulations investigating the sensitivity of the Devonian climate system to various parameters. Settings for the continental configuration, the solar constant  $S$ , the atmospheric  $\text{CO}_2$  concentration, the vegetation distribution, the obliquity  $\varepsilon$  of Earth's axis, the eccentricity  $e$  of its orbit and the precession angle  $\omega$  are listed for all simulations.

the ocean general circulation model MOM3 (Pacanowski and Griffies, 1999; Hofmann and Morales Maqueda, 2006) used at a horizontal resolution of  $3.75^\circ \times 3.75^\circ$  with 24 vertical levels. The coupled model further includes a dynamic/thermodynamic sea-ice model (Fichefet and Morales Maqueda, 1997) operated at the resolution of the ocean model, and a fast statistical-dynamical atmosphere model (Petoukhov et al., 2000) with a coarse spatial resolution of  $22.5^\circ$  in longitude and  $7.5^\circ$  in latitude.

5 All simulations are integrated for 4,000 model years until climate equilibrium is approached.

## 2.2 Boundary conditions and design of the numerical experiments

The main aim of this study is to investigate the sensitivity of Earth's climate system to changes in continental configuration, orbital parameters as well as vegetation distributions and to provide "best-guess" simulations for the Early, Middle and Late



Devonian which are based on the most likely boundary conditions in terms of the distributions of continents and vegetation, the solar constant and the atmospheric carbon-dioxide levels. The design of all experiments is briefly described in the following and summarised in Table 1. In order to facilitate comparisons, we keep as many boundary conditions as possible fixed for the different sensitivity tests. All sensitivity experiments (except for the best-guess simulations) are therefore run with a fixed carbon dioxide concentration of 1500ppm (Foster et al., 2017), and a solar constant of  $S = 1319.1 \text{ Wm}^{-2}$  representative of the Middle Devonian around 380Ma, based on a present day-solar constant of  $S_0 = 1361 \text{ Wm}^{-2}$  (Kopp and Lean, 2011) and a scaling according to a standard solar model (Bahcall et al., 2001).

### 2.2.1 Continental configurations

To test the influence of the continental configuration on the Devonian climate, we set up three model runs with idealised orbital parameters (obliquity  $\varepsilon = 23.5^\circ$ , eccentricity  $e = 0$ ) and use continental configurations representing the Early Devonian (415 Ma), Middle Devonian (380 Ma) and Late Devonian (360 Ma) based on reconstructions (Scotese, 2014). The three different Devonian continental configurations, shown in Fig. 2, are characterised by an arrangement of the continents' largest fraction in the Southern Hemisphere and no land northward of  $60^\circ\text{N}$ . Throughout the Devonian, the most significant changes affect the distribution of land and ocean areas around the South Pole. For our sensitivity experiments with respect to these three Devonian continental configurations it is assumed that there are no land plants, i.e. the land surface type is set to bare land throughout, see Table 1.

### 2.2.2 Vegetation distributions

The biogeophysical influence of spreading vascular land plants is investigated by different (idealised) distributions of vegetation. These are roughly representative of the situation during the Early, Middle and Late Devonian (and will thus be also used in the best-guess simulations described in Section 2.2.4). The sensitivity experiments with respect to the effect of vegetation cover alone, however, use the continental configuration of 360Ma to isolate the biogeophysical effect of vegetation cover from the changes due to the continental configuration.

For the very Early Devonian, we assume that there are only very few land plants; therefore, the land surface type in the model is set to bare land throughout.

By the Middle Devonian, the first vascular land plants had colonised the continents, but these early land plants had shallow roots and could therefore only grow close to water. Thus, we simulate vegetation as grass (shrub) vegetation close to the coast for the Middle Devonian. Specifically, we assume 80% grass-like vegetation cover in areas lower than 500m in altitude and closer than 500km to the coast. Note that grass has evolved much later in Earth's history and that the grass-like surface type in our model approximates the basic biogeophysical properties of any shrub-like vegetation.

For the Late Devonian, we add more widespread vegetation including trees. For this model set-up, coastal areas lower than 500m in altitude and closer than 500km to the coast are covered by 60% of grass and 20% of trees, areas up to 1,500m in altitude and between 500 and 1,000km distance from the coast by 40% grass and 40% trees, and areas with a maximum elevation of 1,500m and a coastal distance between 1,000km and 1,500km by 30% grass and 30% trees.



Part of the biogeophysical effect of vegetation on climate is mediated through changes in surface albedo. For reference, the surface albedo values of the different land surface types (not covered by ice or snow) in our model are 0.14 (visible) and 0.22 (infrared) for bare soil (roughly representative of volcanic soil, Tsvetsinskaya et al. 2002), 0.080 (visible) and 0.30 (infrared) for shrubs, and 0.050 (visible) and 0.20 (infrared) for trees.

- 5 All sensitivity simulations for the different vegetation distributions are run for a fixed carbon dioxide concentration of 1500 ppm, a solar constant of  $S = 1319.1 \text{ Wm}^{-2}$  and idealised orbital configurations, see also Table 1.

### 2.2.3 Orbital parameters

- To find out how changing orbital configurations influence climate, a large set of 51 simulations is performed for obliquity values  $\varepsilon$  of  $22.0^\circ$ ,  $23.5^\circ$ ,  $24.5^\circ$ , eccentricity values  $e$  of 0, 0.03, 0.069, and perihelion angles  $\omega$  (defined relative to autumnal equinox) ranging from  $0^\circ$  to  $315^\circ$  in intervals of  $45^\circ$  for non-zero eccentricity. All other boundary conditions are held fixed at a continental configuration representing 380 Ma, a solar constant of  $S = 1319.1 \text{ Wm}^{-2}$ , a carbon dioxide concentration of 1500 ppm and bare land, see Table 1. Note that our simulations are equilibrium simulations, i.e. we do not simulate transient changes through the Milankovitch cycles.

### 2.2.4 Best-guess simulations

- 15 Finally, for the Early, Middle and Late Devonian we perform a set of three best-guess simulations, representing the most likely state of the variables for the appropriate timeslice. Orbital parameters are set to idealised values (obliquity  $\varepsilon = 23.5^\circ$ , eccentricity  $e = 0$ ), see Table 1.

- For the Early Devonian ( $410 \pm 5 \text{ Ma}$ ), we use the continental configuration of 415 Ma, a carbon dioxide concentration of 2000 ppm and vegetation simulated as bare land. The evolution of land plants is taken into account for the Middle Devonian simulation ( $385 \pm 5 \text{ Ma}$ ) by modeling vegetation only close to coasts as grasses as described in Section 2.2.2. The continental configuration is representative for 380 Ma and the carbon dioxide concentration is set to 1500 ppm. For the Late Devonian ( $365 \pm 5 \text{ Ma}$ ), we use the continental configuration of 360 Ma, vegetation is spread globally with defined fractions of grasses and trees (see Section 2.2.2), and carbon dioxide concentrations are decreased to 1000 ppm.

- 25 The  $\text{CO}_2$  concentrations used are an average value for the represented time period and lie within one standard deviation of the  $\text{pCO}_2$  probability maximum given in Foster et al. (2017), see Fig. 1a.

The solar constant is adjusted for each Devonian timeslice based on the best estimate (Kopp and Lean, 2011) for the present-day solar constant of  $1361 \text{ Wm}^{-2}$  and standard solar evolution (Bahcall et al., 2001), yielding values of  $1315.3 \text{ Wm}^{-2}$ ,  $1319.1 \text{ Wm}^{-2}$  and  $1321.3 \text{ Wm}^{-2}$  for the Early, Middle and Late Devonian, respectively.

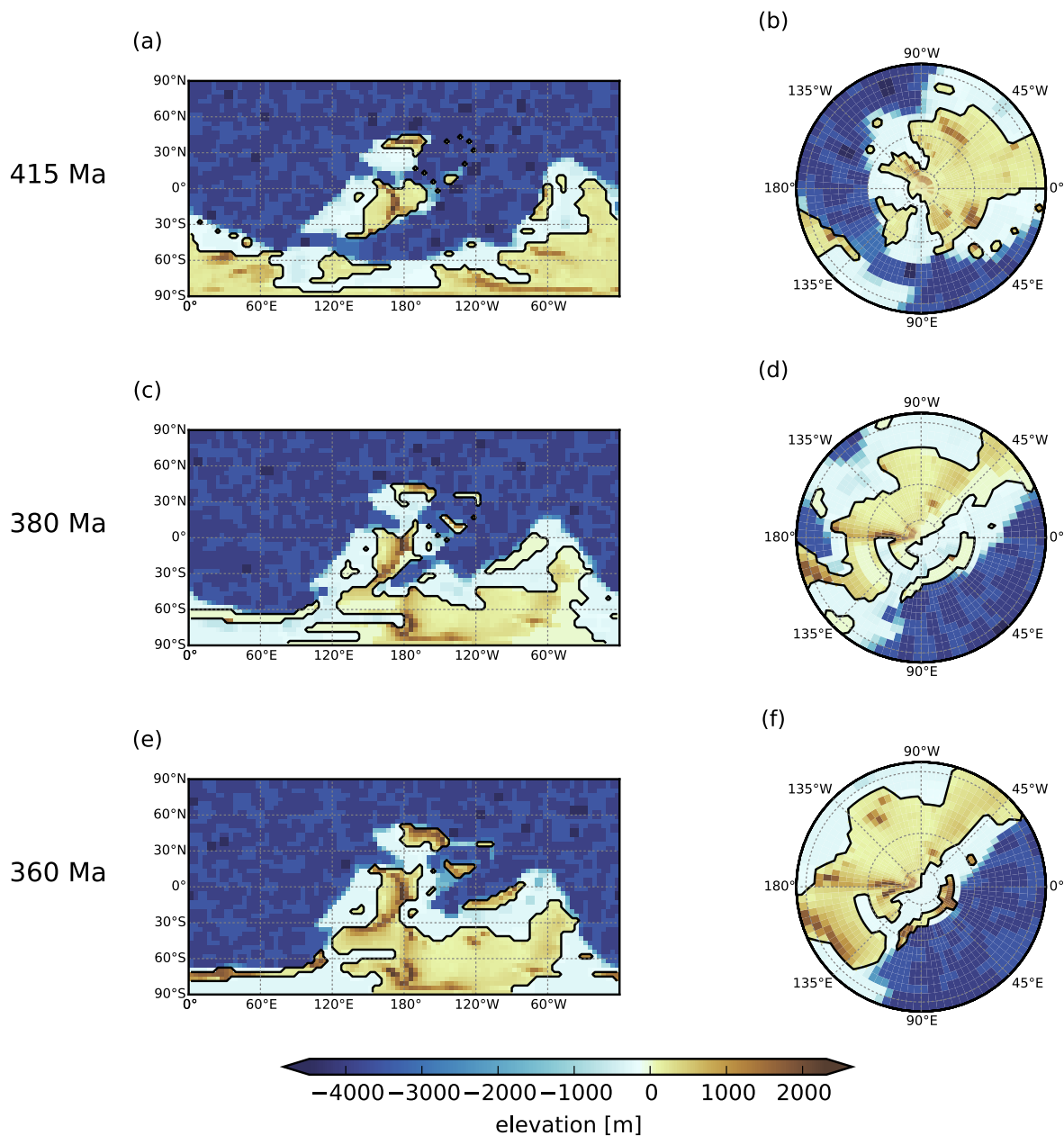


**Figure 2.** Continental configuration, ocean depth and elevation for the three Devonian timeslices at the spatial resolution of our ocean model. Left: Global maps. Right: South Polar view, from 30°S to 90°S. (a) and (b): 415Ma. (c) and (d): 380Ma. (e) and (f): 360Ma.



### 3 Results

#### 3.1 Influence of continental configuration

First we investigate the sensitivity of the Devonian climate to changes in continental configuration while keeping all other boundary conditions fixed ( $\text{CO}_2$  concentration 1500ppm, solar constant  $1319.1 \text{ Wm}^{-2}$ , bare land, idealised orbital parameters; see Table 1 and Section 2.2.1). We compare three simulations using the continental configurations shown in Fig. 2 and find that the change in the distribution of continents throughout the Devonian leads to a decrease of global annual mean surface air temperature over time. However, the temperature differences between the climate states for the three continental configurations are small: for the Early Devonian, global annual mean surface air temperature is  $21.3^\circ\text{C}$ , decreasing to  $21.2^\circ\text{C}$  for the continental configuration of 380Ma and  $20.8^\circ\text{C}$  for 360Ma. While this trend is consistent with the general cooling over the Devonian observed in other modeling and proxy studies, the dominant reason for the general cooling is the decreasing  $\text{CO}_2$  concentration as we will show below (see Section 3.5). Differences in orography between the three timeslices can mostly explain the temperature differences. Furthermore, shifts in the distribution of land and ocean areas as well as changes in ocean circulation likely contribute to the temperature differences.

The influence of the different distribution of land and ocean areas for the three continental configurations are most pronounced in the seasonal temperature differences in the southern high latitudes (see Fig. 3): During southern summer (DJF, maximum solar flux on the South Pole, Fig. 3a), land areas warm faster than ocean areas due to the higher heat capacity of the ocean. In contrast, during southern winter (JJA, minimum solar flux on the South Pole, Fig. 3b), ocean areas are much warmer as they store heat better. As the distribution of land and ocean areas at the South Pole are incongruent when comparing the continental configuration of the Early Devonian with the later ones, we find strong differences in the temperature distribution for the summer months as well as for the winter months for the surface air temperature difference of 360Ma and 415Ma, in agreement with the land-ocean distribution shown in Fig. 2b and f.

#### 3.2 Influence of vegetation

To assess the potential climate impact of the colonisation of the land by vascular plants during the Late Devonian, we investigate the sensitivity of the climate to the biogeophysical effects of different vegetation distributions (bare land, coastal shrub, trees, see Section 2.2.2).

The differences in vegetation do not strongly influence the global mean surface air temperature ( $20.8^\circ\text{C}$  for bare land,  $20.7^\circ\text{C}$  for coastal shrub, and  $20.9^\circ\text{C}$  for trees), but result in regional temperature differences on land. The global mean continental temperature is  $17.2^\circ\text{C}$  for bare land,  $16.4^\circ\text{C}$  for coastal shrub, and  $15.6^\circ\text{C}$  for trees. Figure 4 shows maps of the differences of the coastal shrub and bare land case as well as the differences of the tree and coastal shrub case for surface air temperature, evaporation, surface albedo and atmospheric water content. An analysis of these patterns helps to understand the physical causes of the temperature differences between the different vegetation covers.

Comparing the maps of surface air temperature, evaporation and surface albedo differences, it is evident that differences in evaporation control temperature differences over land for the coastal shrub and bare land case. For the continental temperature

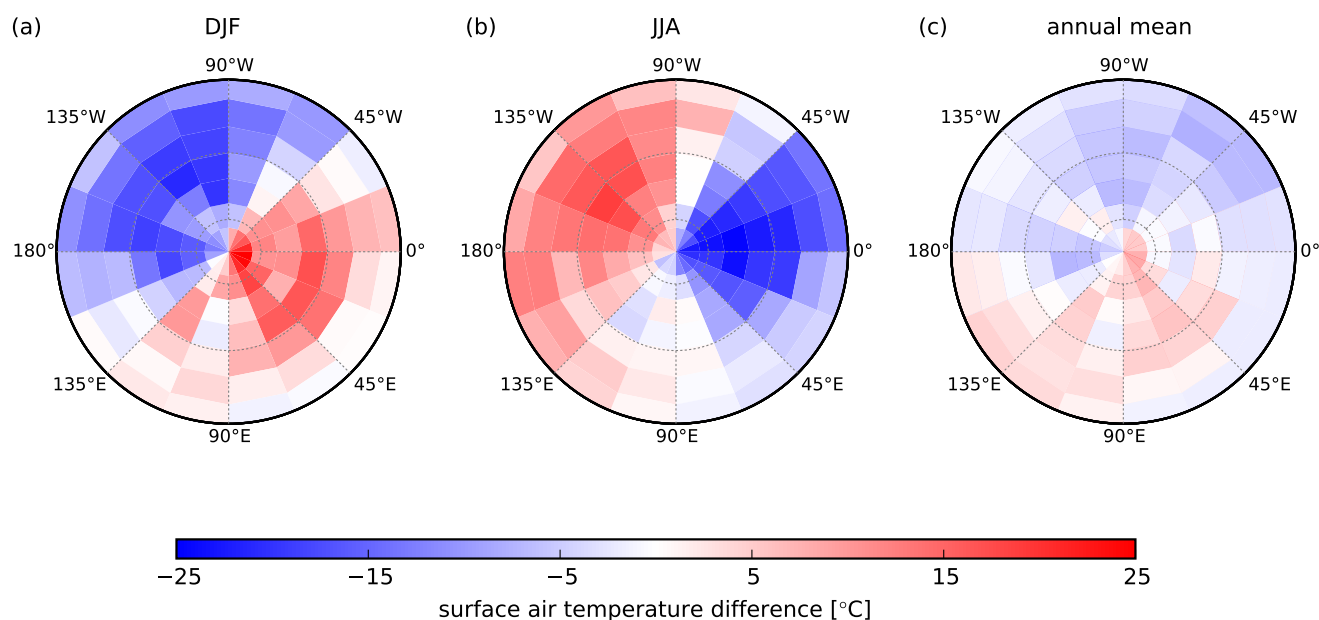


**Figure 3.** Surface air temperature differences between 360Ma and 415Ma in the Southern Hemisphere from 40°S to 90°S. (a) Mean temperature difference for December-January-February (DJF), (b) mean difference for June-July-August (JJA), (c) annual mean difference.

differences of tree and coastal shrub case, this is only the case from the equator to 60°S and on the Northern Hemisphere. Stronger evaporation for grass compared to bare land and for trees compared to coastal shrub results in cooler temperatures. This trend is in agreement with the climatic effect of modern tropical forests (Betts, 2000; Bonan, 2008). The effects of modern temperate forests are very uncertain; for modern boreal forests the negative climate forcing of evaporation is counteracted by the low albedo (Betts, 2000; Bonan, 2008). In the Devonian, continents are covered by snow at higher southern latitudes which reduces differences in evaporation, and therefore albedo differences control differences in temperature: continental temperatures are higher for the tree case for high southern latitudes.

Ocean temperatures are warmer for the tree than for the coastal shrub case. The atmospheric water content of the atmosphere is increased for the tree case compared to the coastal shrub case (Fig. 4 g and h). Although this is a global trend, it dominates surface air temperature differences only for oceanic regions: it leads to an increased greenhouse effect, resulting in higher surface air temperatures. For the continental regions, this effect is counteracted by the evaporative cooling described above. The atmospheric water content difference also determines oceanic surface air temperature difference for the coastal shrub minus bare case. However, in this case, the atmospheric water content is increased by coastal shrub over continents and the ocean in the Southern Hemisphere. In contrast, an increase over the ocean in the Northern Hemisphere is not found. We attribute this to the weaker influence of shrub-like vegetation on evaporation.



In the following we will compare these results with an earlier modelling study. Le Hir et al. (2011) investigate the late Devonian climate using a coupled climate-carbon-vegetation model focusing on the impact of changing surface properties on climate. Similarly to our approach, they use three representative settings for the Early, Middle and Late Devonian. As forcing, they use the solid Earth degassing rate, continental configurations and an increasing solar constant. Although they simulate a strong decrease in CO<sub>2</sub> (5144 ppm for the Early Devonian, 4843 ppm for the Middle Devonian and 2125 ppm for the Late Devonian), they find an almost unchanged temperature of 23.4°C and 23.5°C for the Early and Middle Devonian and, considering the strong CO<sub>2</sub> decrease, the temperature decrease to 22.2°C for the Late Devonian is small. They conclude that the decrease in albedo accompanying the evolution of land plants is counteracting the carbon dioxide decrease. In contrast to our simulations, however, they use relatively high values for the bare soil albedo (0.24 vs. 0.14 in the visible and 0.40 vs. 0.22 in the infrared), whereas their albedo values for vegetation differ only marginally from ours.

To investigate the impact of the choice of albedo for the different surface types, we repeat our three vegetation simulations with the albedo values used in Le Hir et al. (2011). The higher albedo values, and in particularly the significantly higher bare soil albedo, result in reduced temperatures and increased differences between the bare, coastal shrub and tree simulation. Indeed, the bare soil simulation is now the coldest one (18.8°C), followed by the coastal shrub (19.2°C) and tree (20.1°C) simulation. The comparison with our original vegetation simulation results illustrates how strongly the modeled climate impact of differences in vegetation is determined by the choice of albedo values. We note that the soil albedo value used in Le Hir et al. (2011) is comparatively high whereas our choice is relatively low; the two studies therefore effectively sample the plausible range of the albedo effect. Depending on the land albedo before colonisation by vascular plants, albedo changes due to spreading vegetation during the Devonian could therefore have counteracted the CO<sub>2</sub> decrease to some degree. Note, however, that albedo might in reality not have changed too much due to the presence of microbial mats (Boyce and Lee, 2017).

It is important to bear in mind that, in addition to this biogeophysical effects, changes in the weathering process due to the evolution of deeper roots strongly influence the carbon cycle and therefore climate. Hence, these results only give a rough idea of the influence of the land plant evolution on climate, the combined effect of vegetation distribution and decreased CO<sub>2</sub> concentration is discussed in the context of the best-guess simulations, described in Section 3.5.

### 3.3 Influence of orbital configuration

As a third sensitivity test, we investigate the influence of orbital configuration on the Devonian climate using simulations for a range of different orbital parameters while keeping all other boundary conditions fixed (continental configuration for 380 Ma, carbon dioxide concentration 1500 ppm, solar constant 1319.1 Wm<sup>-2</sup>, bare land). In these simulations, we systematically test different values for the obliquity ( $\epsilon = 22.0^\circ$ ,  $23.5^\circ$  and  $24.5^\circ$ ), the eccentricity ( $e = 0$ , 0.03, 0.069) and precession ( $\omega$  from 0 to 315°), see Section 2.2.3.

Figure 5 shows global annual mean surface air temperatures for the three fixed obliquity values when varying eccentricity and precession values. Global annual means of surface air temperature increase with increasing obliquity. For fixed values of  $e = 0$  and  $\omega = 0$ , its values are 21.0°C for  $\epsilon = 22.0^\circ$ , 21.2°C for  $\epsilon = 23.5^\circ$ , and 21.4°C for  $\epsilon = 24.5^\circ$ . Increased obliquity increases seasonal radiation differences on both hemispheres. Although this does not influence annual and global mean values

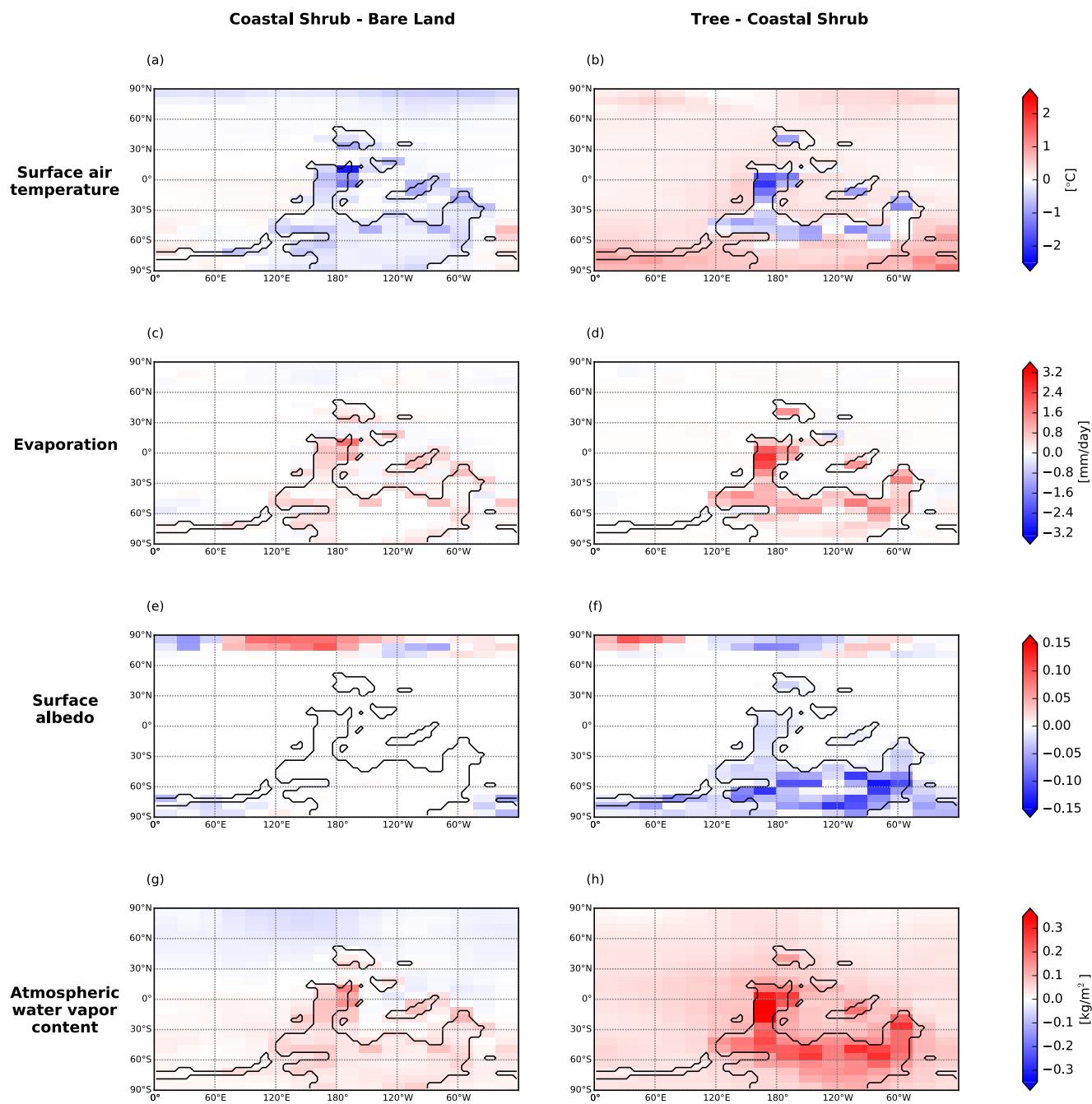


**Figure 4.** Differences of surface air temperature (a, b), evaporation (c, d), surface albedo (c, d) and atmospheric water vapor content (e, f) for climate states with different vegetation cover. Left-hand panels: coastal shrub minus bare land, right-hand panels: tree minus coastal shrub.



of solar radiation, the strong southward shift of the continents amplifies the stronger seasonal insolation at the South Pole for higher obliquity values, resulting in higher global annual mean surface air temperatures.

Concerning the influence of the shape of Earth's elliptical orbit on the Devonian climate, global annual mean surface air temperatures increase with eccentricity due to the higher annual mean insolation for more eccentric orbits. Surface air temperature differences for different precession angles are negligible in our sensitivity experiments.

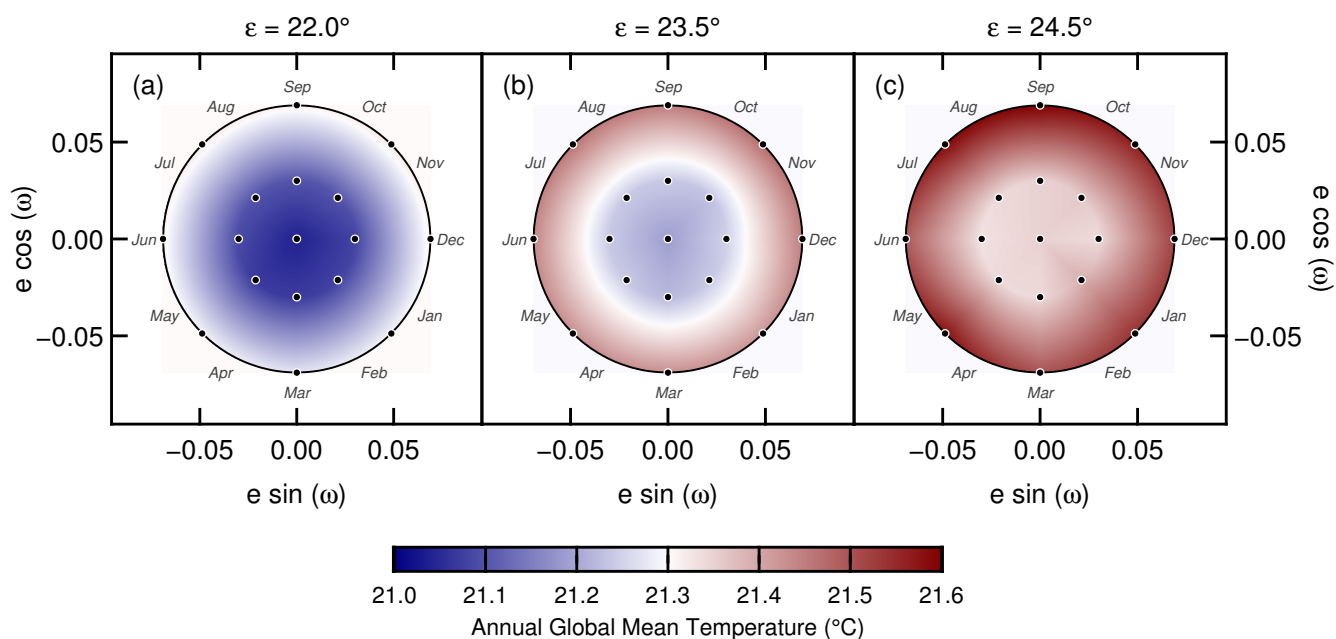


**Figure 5.** Annual global mean surface air temperature for three different obliquities – (a)  $\epsilon = 22.0^\circ$ , (b)  $\epsilon = 23.5^\circ$ , (c)  $\epsilon = 24.5^\circ$  – and varying eccentricity and precession. Note that for each obliquity 17 individual simulations for three different eccentricity values and eight precession angles in intervals of  $45^\circ$  were performed (marked by the black dots); temperatures for all other eccentricity and precession values were derived using bilinear interpolation.

We can compare our results with an earlier modeling study on the impact of orbital parameters on the Devonian climate (De Vleeschouwer et al., 2014) using an atmospheric general circulation model coupled to a slab ocean model with a fixed prescribed oceanic heat transport, a Late Devonian continental configuration, a solar constant of  $1324 \text{ W m}^{-2}$  and a  $\text{CO}_2$  concentration of 2180 ppm. Note that both these values are higher than the ones used in our simulations.

10 Except for a small eccentricity offset of the coldest state and a slight dependence on precession, De Vleeschouwer et al. (2014) also find that global mean temperature increases with obliquity and eccentricity. However, they report significantly larger temperature variations with orbital parameters. Indeed, their coldest state for low obliquity and eccentricity has a global mean temperature of  $19.5^\circ\text{C}$  ( $1.5^\circ\text{C}$  lower than our value for corresponding orbital parameters), while their warmest state for high obliquity and eccentricity has a temperature of  $27^\circ\text{C}$  values (more than  $5^\circ\text{C}$  higher than the warmest state in our



simulations). This discrepancy can be mostly attributed to the slab ocean model used by De Vleeschouwer et al. (2014), since their model uses the same prescribed ocean heat transport for all orbital configurations. In our simulations including ocean dynamics, we find that meridional ocean heat transport largely compensates for seasonal and regional differences in insolation caused by changes in orbital parameters.

- 5 Note that the differences in climate between orbital configurations might be larger in reality than in our idealised simulations at fixed carbon dioxide levels due to feedbacks involving the carbon cycle.

### 3.4 Flips between two climate states in the Arctic

The dominant mode of variability on centennial timescales in our model simulations of the Devonian climate relates to quasi-periodic variations in the global mean surface temperature on the order of  $0.2^{\circ}\text{C}$  with an average periodicity of about 300 years.

- 10 As an example, Fig. 6a shows these variations for a representative time period in one of our sensitivity simulations. These fluctuations in global mean temperature originate from the Arctic region where they are driven by the pace of North Polar sea surface temperature (SST) changes. Indeed, the values of annual mean surface air temperatures regionally averaged over the Arctic between  $60^{\circ}\text{N}$  and  $90^{\circ}\text{N}$  oscillate between about  $3.5^{\circ}\text{C}$  and  $5.0^{\circ}\text{C}$  (Fig. 6b).

- 15 These flips between cold and warm climate states in the Arctic can be attributed to coupled changes in sea-ice cover (shown in Fig. 6b), ocean convection and ocean overturning (Fig. 6c) in the region around the North Pole. A schematic overview of the mechanism is shown in Fig. 7 and described in more detail in the following. During the discussion we will often refer to Fig. 8 where salinity, northern sea-ice cover, ocean surface velocities and the mixed layer depth are shown for the warm mode, the cold mode and the two transition states.

- 20 During the warm mode (Fig. 8a–c) the situation is characterised by the presence of high-salinity surface water at the North Pole, causing a destabilisation of the water column and thus open ocean convection. As a consequence, warmer and saltier water masses are injected into the surface ocean layer while inhibiting the growth of sea ice during the warm mode. Deep ocean convection at the North Pole is, however, intimately connected with the establishment of an Arctic meridional overturning circulation (ArcMOC), see Fig. 6c. The water masses from the surface of the North Pole sink towards the bottom while spreading southward and resurface between  $60^{\circ}\text{N}$  and  $70^{\circ}\text{N}$ .

- 25 While flowing back at sea surface towards the North Pole, the water masses transported by the ArcMOC deliver relatively fresh waters from the latitudinal band between  $70^{\circ}\text{N}$  and  $80^{\circ}\text{N}$ , which promotes the recurrence of sea-ice formation and thus the transition from the warm into the cold mode (Fig. 8d–f). As seasonal sea ice grows, deep convection at the North Pole weakens and ultimately ceases because the layer of sea ice inhibits heat losses from sea surface. As a consequence, the ArcMOC collapses (Fig. 6c) and the system lapses into the cold mode.

- 30 Within the time interval of the cold mode (Fig. 8g–i), the formation of seasonal sea ice in the Arctic leads to a lowering of the sea surface salinity (SSS) around the North Pole caused by the impacts of brine rejection during sea-ice formation and a freshening of sea surface waters during its melting period (Bouttes et al., 2010). Consequently, the cold mode is characterised by a shallow mixed layer and strong stratification of Polar water masses where cold and relatively fresh water lies above warmer

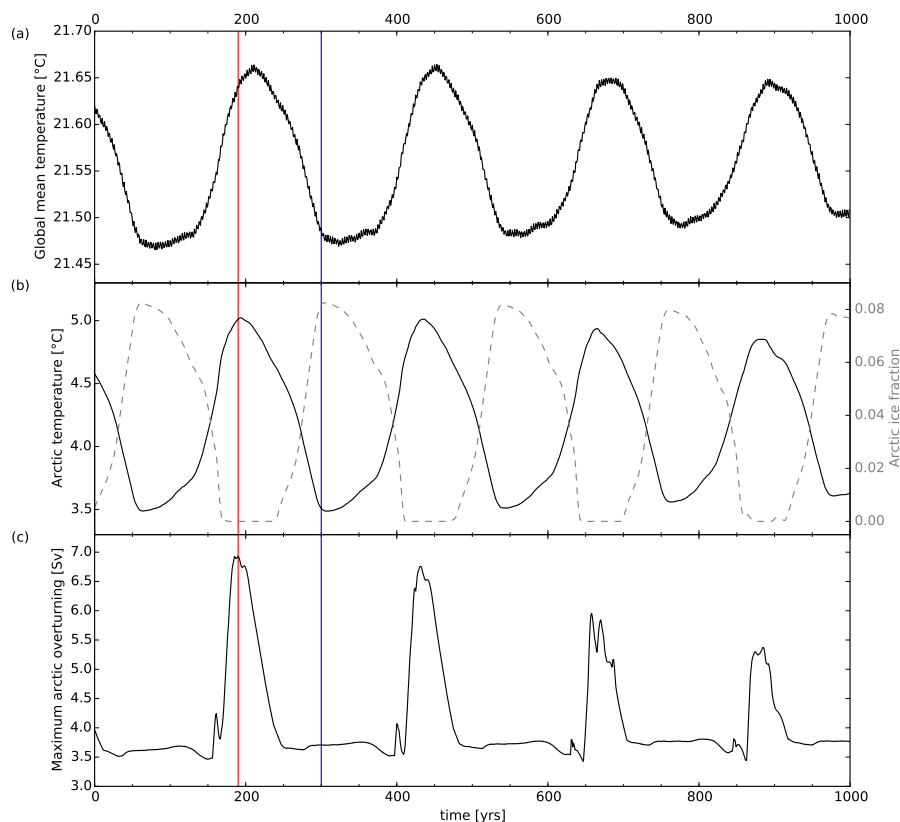


**Figure 6.** Typical mode of climate variability in the Devonian as diagnosed in a representative 1,000-years period of the model simulation for 380Ma, 1500ppm of  $\text{CO}_2$ ,  $S = 1319.1 \text{ Wm}^{-2}$ ,  $\varepsilon = 24.5^\circ$ ,  $e = 0.069$  and  $\omega = 315^\circ$ . (a) Global annual mean surface air temperature. (b) Arctic annual surface air temperature, averaged from  $60^\circ\text{N}$  to  $90^\circ\text{N}$  (black solid line), and Arctic annual sea-ice fraction (grey dashed line). (c) Maximum of the Arctic overturning circulation in the ocean between  $60^\circ\text{N}$  and  $90^\circ\text{N}$  in latitude and between 500m and 3000m depth. The red and blue lines mark the points which are chosen for diagnostic snapshots of the warm and cold mode in the following.

and salty water masses. The surface velocities follow almost a cyclonic flow pattern south of  $60^\circ\text{N}$  and a weaker anticyclonic pattern north of  $70^\circ\text{N}$ , combined with a circularly symmetric shaped dynamical free surface  $\eta$ .

However, due to deviations from perfect circular symmetry of water mass properties around the North Pole, the cold mode is unstable, and the system begins the transition back into the warm mode (Fig. 8j–l). As sea ice forms and melts over the 5 years, the relatively fresh surface water layer accumulating around the North Pole spreads slightly asymmetrically towards the south. Therefore, the concomitant formation of a meandering density front within the latitudinal band between  $60^\circ\text{N}$  and  $80^\circ\text{N}$  reshapes the dynamic free surface  $\eta$  according to the geostrophical balance (Marshall and Plumb, 2008). The resulting deflection of the circular flow from lower latitudes of around  $60^\circ\text{N}$  towards the North Pole drives patches of highly saline surface water masses towards the Pole.

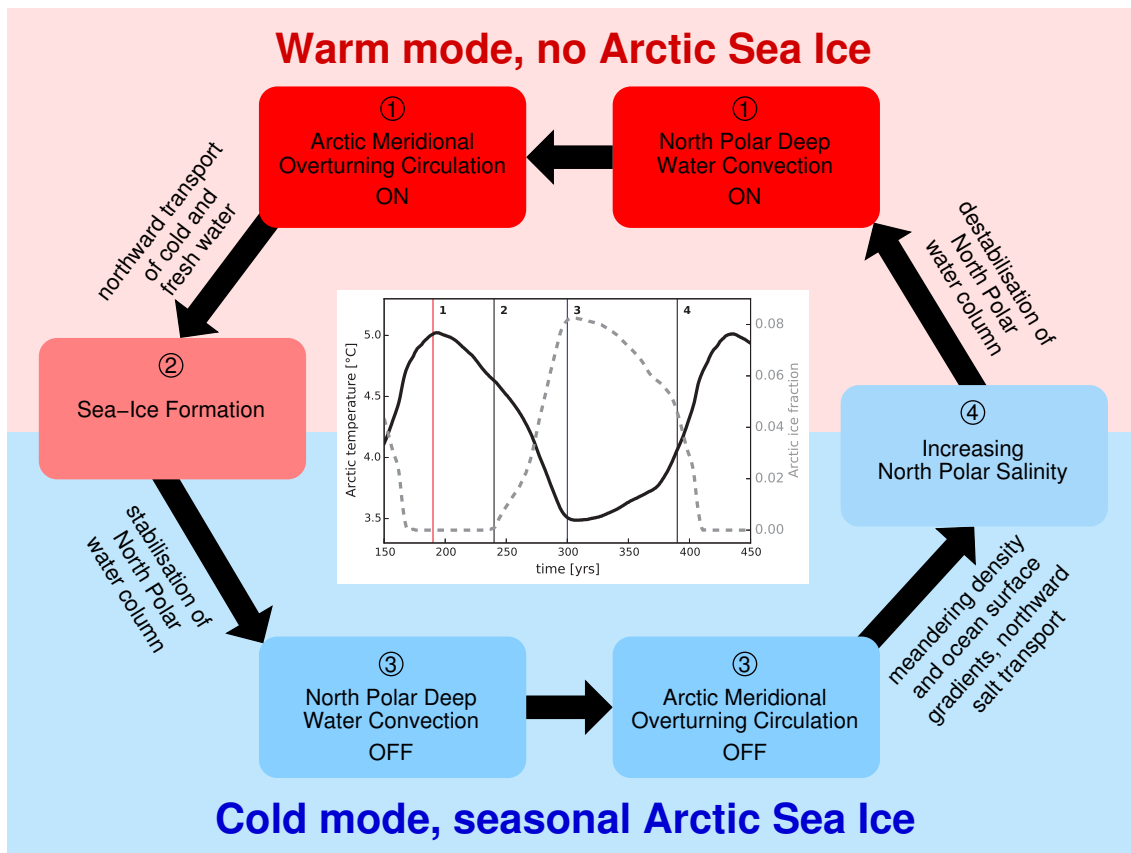


**Figure 7.** Mechanism describing the flip between the two climate states in the Arctic: In the warm mode, the North Polar water column is destabilised by the northbound transport of warmer and saltier waters to the ocean surface. This inhibits the growth of sea ice and is connected to the establishment of a North Polar deep water convection. The accompanying Arctic meridional overturning circulation transports cold and fresh water northward, leading to the flip into the cold mode. The formation of sea ice stops the deep water convection and the Arctic meridional overturning circulation. The resulting meandering density and ocean surface gradients lead to a northbound salt transport, increasing surface salinity at the North Pole and thereby triggering the flip back into the warm mode.

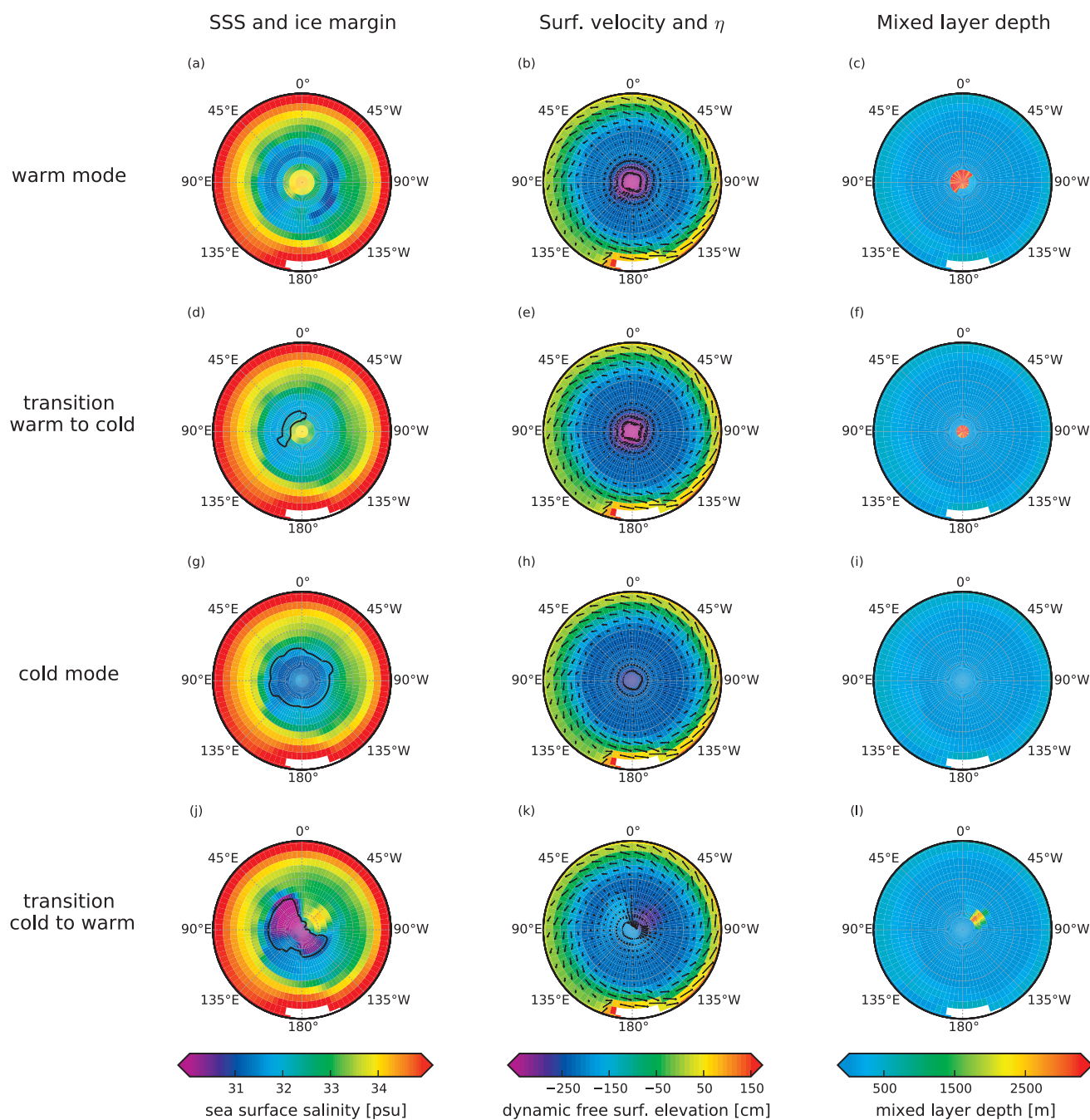


**Figure 8.** Physical properties of the northern-hemisphere ocean between  $40^{\circ}\text{N}$  and the North Pole for the warm mode (first row, a–c), the transition between warm and cold mode (second row, d–f), the cold mode (third row, g–i) and the transition between cold and warm mode (fourth row, j–l). Quantities shown are sea surface salinities (SSS) in psu and the area covered with at least 10% of sea ice during winter as black line (left column, a, d, g, j), dynamic free surface elevation  $\eta$  in cm overlaid by sea surface velocity vectors in  $\text{cm s}^{-1}$  (centre column, b, e, h, k), mixed layer depth in m (right column, c, f, i, l).



This advancing salinification of surface waters at the North Pole ultimately causes a destabilisation of the water column, open ocean convection at the pole and the restart of the ArcMOC, thus switching the system back into the warm mode.

Oscillations like the one described here could in principle also result from numerical instabilities caused by a long simulation timestep (12 h by default), the splitting of tracer and dynamic timesteps employed in our ocean model (Montoya et al., 2005) or  
5 by rounding errors due to optimisation during code compilation. We have performed a large set of test experiments including simulations with short timesteps (as low as 1 h) and without splitting of ocean timesteps, experiments on different platforms and with different compiler versions and optimisation settings to verify that the oscillations described above are a real phenomenon rather than a numerical artefact.

Our results suggest that similar modes of climate variability could be a more general feature of climate states with open  
10 water at one pole provided that the global energy balance allows this pole to be seasonally free of sea-ice.

### 3.5 Best-guess simulation for each timeslice

After having investigated the sensitivity of the Devonian climate state to single parameters, we finally perform best-guess simulations with the aim to represent the most likely state for the three times periods of the Early, Middle and Late Devonian by choosing the most appropriate combination of parameter values (Table 1), as explained in Section 2.2.4. Simulated surface  
15 air temperature decreases significantly throughout the Devonian: During the Early Devonian, global annual mean surface air temperature is 22.2°C, decreasing to 21.0°C for the Middle Devonian and 19.3°C for the Late Devonian.

The global cooling over the Devonian seen in the set of best-guess simulations only partly reflects the observed trend of decreasing temperatures caused purely by changes in the continental configurations (see Section 3.1), but is dominantly driven by the strong decrease in CO<sub>2</sub> concentrations which are reduced by a factor of two from the Early Devonian to the Late  
20 Devonian. In contrast, the solar constant increased throughout the Devonian and therefore partly counteracted the cooling caused by the decreased CO<sub>2</sub> concentration. The influence of differences in vegetation cover, as described in Section 3.2, can be neglected compared to the temperature changes induced by the change in CO<sub>2</sub> concentration and solar constant.

Regional surface air temperatures are shown in Fig. 9. One of the more prominent features on these maps is a warm region in the tropics around 180° in longitude on the western continental margin, which is most pronounced for the Early Devonian  
25 simulation (see Fig. 9a). This warm patch with increased precipitation (not shown) is connected to the orographic features of the Laurussian continent: The mountain range in the continent's interior influences atmospheric circulation and intensifies and enlarges the intertropical convergence zone's low-pressure areas. On the mountains' eastern margin, humid air is transported from the ocean and leads to increased precipitation which results in an increase in latent heat.

In their modeling study investigating the impact of orbital forcing on the Devonian climate (see Section 3.3) De Vleeschouwer  
30 et al. (2014) also provide maps of DJF and JJA surface temperatures for a Late Devonian median orbit ( $\epsilon = 23.5^\circ$  and  $e = 0$ ) climate simulation. Keeping in mind that they use higher values for the CO<sub>2</sub> concentration and the solar constant, the patterns agree well with our Late Devonian simulation.

In the following we compare temperatures derived from our best-guess simulations with available proxy data. Several studies determine tropical sea surface temperatures (SSTs) using  $\delta^{18}\text{O}$  from proxy data. van Geldern et al. (2006) use  $\delta^{18}\text{O}$  brachiopod

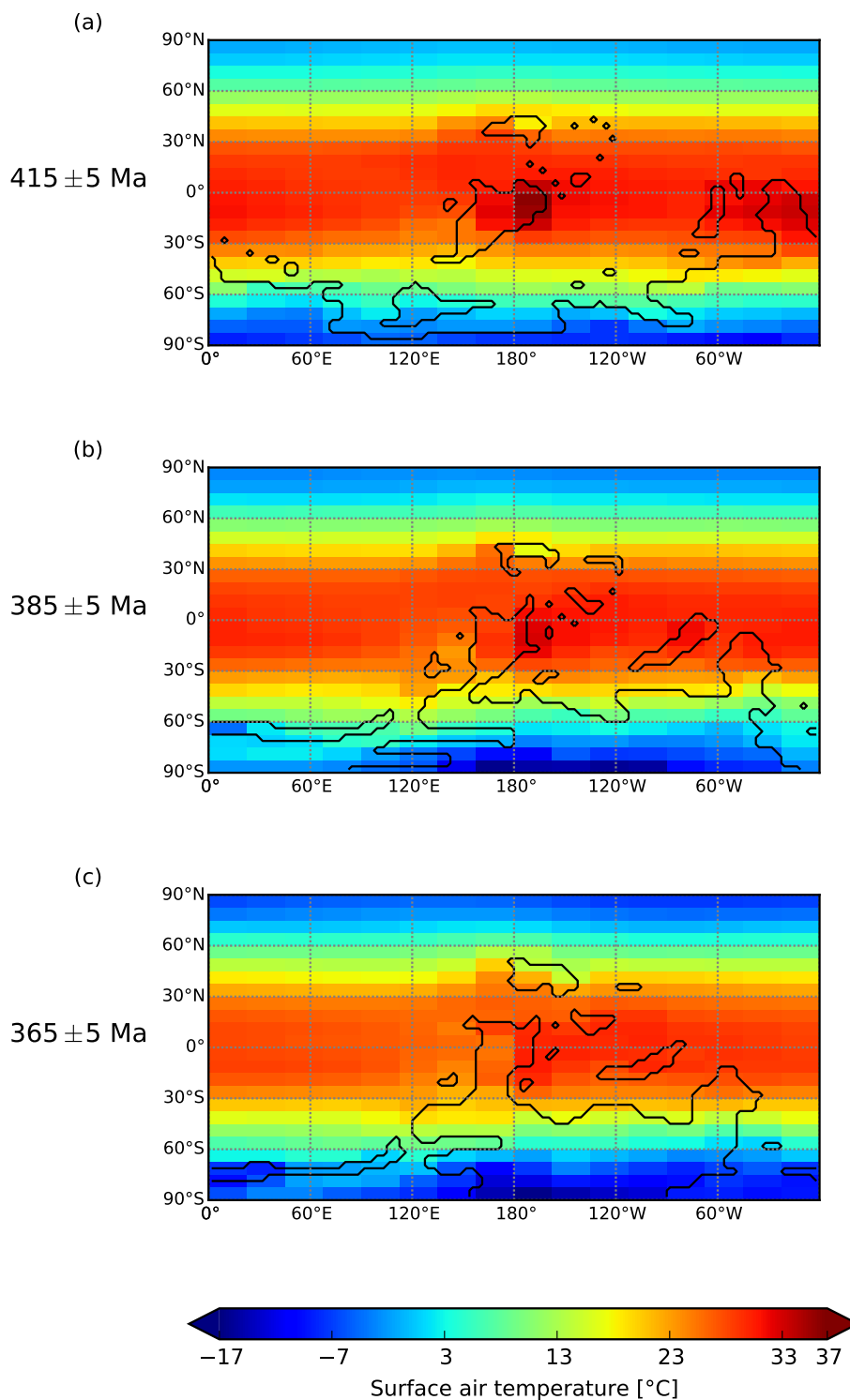


**Figure 9.** Maps of annual mean surface air temperatures for the best-guess simulations of the climate during the Early Devonian (a), Middle Devonian (b) and Late Devonian (c).



shells to derive SSTs ranging from 24 to 27°C in tropical to subtropical latitudes for the Early and Middle Devonian. For the Late Devonian, they discuss that their temperature estimates of 31 to 41°C are significantly too warm for providing good living conditions for the diverse marine life found in their investigated successions, possibly suggesting an increase in  $\delta^{18}\text{O}$  of seawater (Jaffrés et al., 2007) between the Devonian and the present-day.

5 Joachimski et al. (2009) point out difficulties in the interpretation of  $\delta^{18}\text{O}$  brachiopod shell signals and provide a  $\delta^{18}\text{O}$  record from conodonts (see Fig. 1b) which they argue to be a more reliable palaeotemperature record. In Fig. 10 we compare their tropical SST estimates for different calibration standards and temperature equations with the SSTs from our best-guess simulations. For the Early Devonian, the new SST curve (M. Joachimski, priv. comm.) based on a temperature equation leading to high temperature estimates shows warm SSTs of 35 to 37°C, with a cooling trend, continuing in the Middle Devonian, to 10 temperatures of 23 to 27°C. This is followed by an increase to 36°C in the early Late Devonian and a slight decrease to 30°C towards the end of the Devonian.

Except for the Middle Devonian, the modelled temperatures from our best-guess simulations also shown in Fig. 10 generally compare better with the lower SSTs values given in Joachimski et al. (2009) rather than the SSTs calculated using the new calibration standard and temperature curve (Lécuyer et al., 2003, 2013). Together with the fact that these very high SSTs are 15 beyond the mortality limit for diverse marine life (van Geldern et al., 2006) this could indicate lower  $\delta^{18}\text{O}$  levels of Devonian ocean water as compared to the present-day ocean (Jaffrés et al., 2007).

Concerning comparison of our results with earlier modelling studies, global annual mean surface air temperatures for the best-guess simulations using the albedo values of Le Hir et al. (2011) are lower than our standard best-guess simulations with 20.5°C for the Early, 19.9°C for the Middle and 18.5°C for the Late Devonian. However, in contrast to the simulations 20 of Le Hir et al. (2011), we still simulate temperatures decreasing by 2°C from the Early to the Late Devonian. Therefore, even for high bare-soil albedo values, the effect of a decreasing albedo caused by the evolution of land plants is not strong enough to counteract the cooling effect of the decreasing  $\text{CO}_2$  as suggested by Le Hir et al. (2011). Hence, like other modeling studies (Simon et al., 2007), our model results do not support the higher temperatures of the late Frasnian and early Famennian compared to the Middle Devonian, suggested by SST proxy data (Joachimski et al., 2009; van Geldern et al., 2006) and 25 palaeontological studies (Streel et al., 2000).

Simon et al. (2007) investigate the evolution of the short-term atmospheric  $\text{CO}_2$  concentration during the Devonian using a global biogeochemical model coupled to an energy-balance climate model, taking into account the changes in continental configuration, sea-level changes and the increase of vegetation covered by land plants. The modeled  $\text{CO}_2$  concentration of 3000 ppm for the Early Devonian is very high (see Fig. 1) and shows a general decreasing trend throughout the Devonian going 30 along with the evolution of land plants, reaching low concentrations of 1000 ppm already around 390 Ma and then fluctuating around this value during the following 30 million years. For the three Devonian periods covered by our best-guess simulations, the low-latitude temperatures of Simon et al. (2007) compare well with their equivalent in our simulations although both studies are based on very different modelling approaches.

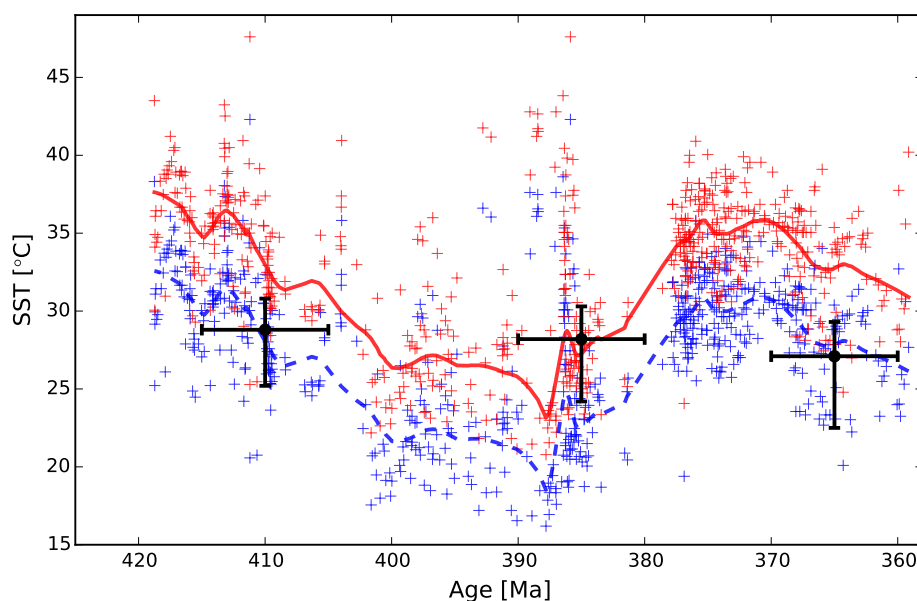


**Figure 10.** Comparison of reconstructed and modelled tropical sea-surface temperatures for the Devonian. The blue crosses represent temperature estimates based on  $\delta^{18}\text{O}$  data as shown in Joachimski et al. (2009); the red crosses (M. Joachimski, priv. comm.) are based on the same data, but use an updated NBS120c calibration standard of 21.7 (Lécuyer et al., 2003) rather than 22.6 (Vennemann et al., 2002) and assume a different temperature equation (Lécuyer et al., 2013). The solid red and dashed blue lines show local regression fits to the data points. The filled black circles are modelled SSTs from our best-guess simulations averaged from 10 to 30°S since all the sections used for the temperature reconstruction in Joachimski et al. (2009) are located at palaeolatitude in this range. The uncertainty bars in age ( $\pm 5$  Ma) indicate the approximate age intervals for which our best-guess simulations can be considered representative given their continental configuration and  $\text{CO}_2$  concentration; the lower and upper end of the temperature ranges in the model are based on the average SSTs at latitudes of 30°S and 10°S, respectively.

#### 4 Conclusions

In a first attempt to disentangle the various factors influencing Earth's climate during the Devonian, we have systematically performed and analysed a large set of sensitivity simulations with a coupled climate model, focussing in particular on the impact of changes in continental configuration, the biogeophysical effects of increasing vegetation cover and variations related to Earth's orbital parameters. The key findings of our paper can be summarised as follows:

1. The impact of changes in orbital parameters (at a fixed  $\text{CO}_2$  concentration) on the climate is in line with the findings of De Vleeschouwer et al. (2014) in the sense that annual global mean temperature increases with obliquity and eccentricity. However, the differences in global mean temperature are much smaller in our simulations using an ocean general circulation model (rather than a simple ocean model with fixed heat transport) because of changes in ocean heat transport counteracting the insolation changes.



2. The most important mode of Devonian climate variability on centennial timescales relates to coupled changes in Arctic meridional ocean overturning, northern sea-ice cover and deep ocean convection around the North Pole. We suggest that this mode of climate variability is a more general feature of climate states with open water at one pole as long as the energy balance allows that this pole is seasonally free of sea-ice.
- 5 3. “Best-guess” simulations based on estimates of continental configuration, vegetation cover, solar constant and atmospheric carbon-dioxide concentration for three timeslices approximately representing the Early, Middle and Late Devonian show a general climatic cooling trend in accordance with reconstructions showing decreasing levels of atmospheric CO<sub>2</sub> concentrations during the Devonian. Furthermore, the biogeophysical impact of an increasing vegetation cover on the Devonian climate is small. In particular, the associated albedo changes cannot completely compensate for the falling  
10 CO<sub>2</sub> concentrations (unlike suggested in Le Hir et al. 2011) even under the assumption of a relatively high bare-soil albedo. The increase in temperatures around 390Ma observed in reconstructions therefore remains difficult to reconcile with CO<sub>2</sub> estimates.
- 15 4. Finally, simulated tropical sea-surface temperatures for our Devonian timeslices are generally significantly lower than the estimates based on  $\delta^{18}\text{O}$  and the latest temperature calibration. This discrepancy and the fact that reconstructed temperatures are at times beyond the lethal limit for higher life (van Geldern et al., 2006) could indicate a general difference in the oxygen isotope ratio between the Devonian and modern oceans.

Our results on the Devonian climate highlight that much remains to be done to improve our understanding of this crucial period. Open issues include a better quantification of the biogeochemical impact of the spread of vascular land plants, the puzzling warming at the beginning of the Late Devonian despite falling atmospheric carbon-dioxide levels and the interplay  
20 between terrestrial changes and the marine extinction events.

*Code and data availability.* The source code for the model used in this study, the data and input files necessary to reproduce the experiments, and model output data are archived at the Potsdam Institute for Climate Impact Research and are made available upon request.

*Author contributions.* JB and GF designed the study, all authors carried out and analysed model simulations, JB and GF wrote the paper with input from MH and SP.

25 *Competing interests.* The authors declare that they have no conflict of interest.



*Acknowledgements.* We thank Christopher Scotese for providing palaeocontinental reconstruction in electronic form, Michael Joachimski for sending their  $\delta^{18}\text{O}$  and temperature data and Jan Wohland for helpful comments. The European Regional Development Fund (ERDF), the German Federal Ministry of Education and Research and the Land Brandenburg are gratefully acknowledged for supporting this project by providing resources on the high performance computer system at the Potsdam Institute for Climate Impact Research. JB acknowledges funding by the German Federal Ministry of Education and Research BMBF within the Collaborative Project “Bridging in Biodiversity Science – BIBS” (funding number 01LC1501A-H).



## References

- Algeo, T. J. and Scheckler, S. E.: Terrestrial-marine teleconnections in the Devonian: links between the evolution of land plants, weathering processes, and marine anoxic events, *Transactions of the Royal Society B: Biological Sciences*, 353, 113–130, <https://doi.org/10.1098/rstb.1998.0195>, 1998.
- 5 Algeo, T. J., Berner, R. A., Barry, M. J., and Scheckler, S. E.: Late Devonian Oceanic Anoxic Events and Biotic Crises: "Rooted" in the Evolution of Vascular Land Plants?, *GSA Today*, 5, 45,64–66, 1995.
- Bahcall, J. N., Pinsonneault, M. H., and Basu, S.: Solar Models: Current Epoch and Time Dependences, Neutrinos, and Helioseismological Properties, *Astrophys. J.*, 555, 990–1012, <https://doi.org/10.1086/321493>, 2001.
- Bambach, R. K.: Phanerozoic biodiversity mass extinctions, *Annu. Rev. Earth Planet. Sci.*, 34, 127–155, <https://doi.org/10.1146/annurev.earth.33.092203.122654>, 2006.
- 10 Berner, R.: GEOCARBII: A revised model of atmospheric CO<sub>2</sub> over Phanerozoic time, *Am J Sci*, 294, 56–91, <https://doi.org/doi:10.2475/ajs.301.2.182>, 1994.
- Berner, R.: GEOCARBSULF: A combined model for Phanerozoic atmospheric O<sub>2</sub> and CO<sub>2</sub>, *Geochim Cosmochim Ac*, 70, 5653–5664, <https://doi.org/10.1016/j.gca.2005.11.032>, a Special Issue Dedicated to Robert A. Berner, 2006.
- 15 Betts, R. A.: Offset of the potential carbon sink from boreal forestation by decreases in surface albedo, *Nature*, 408, 187–190, <https://doi.org/10.1038/35041545>, 2000.
- Bonan, G. B.: Forests and Climate Change: Forcings, Feedbacks, and the Climate Benefits of Forests, *Science*, 320, 1444–1449, <https://doi.org/10.1126/science.1155121>, 2008.
- Bond, D. and Wignall, P.: The role of sea-level change and marine anoxia in the Frasnian-Famennian (Late Devonian) mass extinction, *Palaeogeogr Palaeocl*, 263, 107–118, <https://doi.org/10.1016/j.palaeo.2008.02.015>, 2008.
- 20 Bouttes, N., Paillard, D., and Roche, D. M.: Impact of brine-induced stratification on the glacial carbon cycle, *Climate of the Past*, 6, 575–589, <https://doi.org/10.5194/cp-6-575-2010>, 2010.
- Boyce, C. K. and Lee, J.-E.: Plant Evolution and Climate Over Geological Timescales, *Annu. Rev. Earth Planet. Sci.*, 45, 61–87, <https://doi.org/10.1146/annurev-earth-063016-015629>, 2017.
- 25 Brezinski, D. K., Cecil, C. B., Skema, V. W., and Stamm, R.: Late Devonian glacial deposits from the eastern United States signal an end of the mid-Paleozoic warm period, *Palaeogeogr Palaeocl*, 268, 143–151, <https://doi.org/10.1016/j.palaeo.2008.03.042>, 2008.
- Brezinski, D. K., Cecil, C. B., Skema, V. W., and Kertis, C. A.: Evidence for long-term climate change in Upper Devonian strata of the central Appalachians, *Palaeogeogr Palaeocl*, 284, 315–325, <https://doi.org/10.1016/j.palaeo.2009.10.010>, 2009.
- Caputo, M. V.: Late Devonian Glaciation in South America, *Palaeogeogr Palaeocl*, 51, 291–317, [https://doi.org/10.1016/0031-0182\(85\)90090-2](https://doi.org/10.1016/0031-0182(85)90090-2), 1985.
- 30 Caputo, M. V., de Melo, J. H. G., StreeL, M., and Isbell, J. L.: Late Devonian and Early Carboniferous glacial records of South America, in: *Resolving the Late Paleozoic Ice Age in Time and Space*, edited by Fielding, C., Frank, T., and Isbell, J., chap. 11, [https://doi.org/10.1130/2008.2441\(11\)](https://doi.org/10.1130/2008.2441(11)), 2008.
- Clack, J. A.: Devonian climate change, breathing, and the origin of the tetrapod stem group, *Integrative and Comparative Biology*, 47, 510–523, <https://doi.org/10.1093/icb/icm055>, 2007.



- Copper, P. and Scotese, C.: Megareefs in Middle Devonian supergreenhouse climates, *in* Chan, M.A., and Archer, A.W., eds., Extreme depositional environments: Mega end members in geologic time: Boulder, Colorado, *Geol S Am S*, 370, 209–230, <https://doi.org/10.1130/0-8137-2370-1.209>, 2003.
- Dahl, T. W., Hammarlund, E. U., Anbar, A. D., Bond, D. P. G., Gill, B. C., Gordon, G. W., Knoll, A. H., Nielsen, A. T., Schovsbo, N. H.,  
5 and Canfield, D. E.: Devonian rise in atmospheric oxygen correlated to the radiations of terrestrial plants and large predatory fish, *P Natl Acad Sci USA*, 107, 17 911–17 915, <https://doi.org/10.1073/pnas.1011287107>, 2010.
- De Vleeschouwer, D., Rakocinski, M., Racki, G., Bond, D., Sobień, K., Bounceur, N., Crucifix, M., and Claeys, P.: The astronomical rhythm of Late-Devonian climate change (Kowala section, Holy Cross Mountains, Poland), *Earth Planet Sc Lett*, pp. 25–37, <https://doi.org/10.1016/j.epsl.2013.01.016>, 2013.
- 10 De Vleeschouwer, D., Crucifix, M., Bounceur, N., and Claeys, P.: The impact of astronomical forcing on the Late Devonian greenhouse climate, *Global Planet Change*, 120, 65–80, <https://doi.org/10.1016/j.gloplacha.2014.06.002>, 2014.
- De Vleeschouwer, D., Da Silva, A.-C., Sinnesael, M., Chen, D., Day, J. E., Whalen, M. T., Guo, Z., and Claeys, P.: Timing and pacing of the Late Devonian mass extinction event regulated by eccentricity and obliquity, *Nat Commun*, 8:2268, <https://doi.org/10.1038/s41467-017-02407-1>, 2017.
- 15 Fichfet, T. and Morales Maqueda, M. A.: Sensitivity of a global sea ice model to the treatment of ice thermodynamics and dynamics, *J. Geophys. Res.*, 102, 12 609–12 646, <https://doi.org/10.1029/97JC00480>, 1997.
- Foster, G. L., Royer, D. L., and Lunt, D. J.: Future climate forcing potentially without precedent in the last 420 million years, *Nature Communications*, 8, 14 845, <https://doi.org/10.1038/ncomms14845>, 2017.
- Godderis, Y. and Joachimski, M.: Global change in the Late Devonian: Modelling the Frasnian-Famennian short-term carbon isotope excursions, *Palaeogeogr Palaeoclimatol*, 202, 309–329, 2004.
- 20 Haq, B. U. and Schutter, S. R.: A Chronology of Paleozoic Sea-Level Changes, *Science*, 322, 64–68, <https://doi.org/10.1126/science.1161648>, 2008.
- Hofmann, M. and Morales Maqueda, M. A.: Performance of a second-order moments advection scheme in an Ocean General Circulation Model, *J. Geophys. Res.*, 111, C05 006, <https://doi.org/10.1029/2005JC003279>, 2006.
- 25 Jaffrés, J. B., Shields, G. A., and Wallmann, K.: The oxygen isotope evolution of seawater: A critical review of a long-standing controversy and an improved geological water cycle model for the past 3.4 billion years, *Earth-Sci Rev*, 83, 83–122, <https://doi.org/10.1016/j.earscirev.2007.04.002>, 2007.
- Joachimski, M., Breisig, S., Buggisch, W., Talent, J., Mawson, R., Gereke, M., Morrow, J., Day, J., and Weddige, K.: Devonian climate and reef evolution: Insights from oxygen isotopes in apatite, *Earth Planet Sc Lett*, 284, 599–609, <https://doi.org/10.1016/j.epsl.2009.05.028>,  
30 2009.
- Johnson, J. G., Klapper, G., and Sandberg, C. A.: Devonian eustatic fluctuations in Euramerica, *GSA Bulletin*, 96, 567, [https://doi.org/10.1130/0016-7606\(1985\)96<567:DEFIE>2.0.CO;2](https://doi.org/10.1130/0016-7606(1985)96<567:DEFIE>2.0.CO;2), 1985.
- Kopp, G. and Lean, J. L.: A new, lower value of total solar irradiance: Evidence and climate significance, *Geophys. Res. Lett.*, 38, L01706, <https://doi.org/10.1029/2010GL045777>, 2011.
- 35 Le Hir, G., Donnadiou, Y., Godderis, Y., Meyer-Berthaud, B., Ramstein, G., and Blakey, R. C.: The climate change caused by the land-plant invasion in the Devonian, *Earth Planet Sc Lett*, 310, 203–212, <https://doi.org/10.1016/j.epsl.2011.08.042>, 2011.



- Lécuyer, C., Picard, S., Garcia, J.-P., Sheppard, S. M. F., Grandjean, P., and Dromart, G.: Thermal evolution of Tethyan surface waters during the Middle-Late Jurassic: Evidence from  $\delta^{18}\text{O}$  values of marine fish teeth, *Paleoceanography*, 18, <https://doi.org/10.1029/2002PA000863>, 2003.
- Lécuyer, C., Amiot, R., Touzeau, A., and Trotter, J.: Calibration of the phosphate  $\delta^{18}\text{O}$  thermometer with carbonate–water oxygen isotope fractionation equations, *Chem Geol*, 347, 217–226, <https://doi.org/10.1016/j.chemgeo.2013.03.008>, 2013.
- Ma, X., Gong, Y., Chen, D., Racki, G., Chen, X., and Liao, W.: The Late Devonian Frasnian–Famennian Event in South China — Patterns and causes of extinctions, sea level changes, and isotope variations, *Palaeogeogr Palaeoclimatol*, 448, 224–244, <https://doi.org/10.1016/j.palaeo.2015.10.047>, 2016.
- Marshall, J. and Plumb, R. A.: *Atmosphere, Ocean, and Climate Dynamics: An Introductory Text*, Elsevier Academic Press: International Geophysics Series, Vol. 93, 2008.
- McGhee, G. R., Gilmore, J. S., Orth, C. J., and Olsen, E.: No geochemical evidence for an asteroidal impact at late Devonian mass extinction horizon, *Nature*, 308, 629–631, <https://doi.org/10.1038/308629a0>, 1984.
- Milankovitch, M.: *Kanon der Erdbestrahlung und seine Anwendung auf das Eiszeitenproblem*, Königlich Serbische Akademie, Belgrad, 1941.
- Montoya, M., Griesel, A., Levermann, A., Mignot, J., Hofmann, M., Ganopolski, A., and Rahmstorf, S.: The earth system model of intermediate complexity CLIMBER-3 $\alpha$ . Part I: description and performance for present-day conditions, *Clim. Dyn.*, 25, 237–263, <https://doi.org/10.1007/s00382-005-0044-1>, 2005.
- Pacanowski, R. C. and Griffies, S. M.: *The MOM-3 Manual*, Tech. Rep. 4, GFDL Ocean Group, NOAA/Geophysical Fluid Dynamics Laboratory, Princeton, NJ, 1999.
- Petoukhov, V., Ganopolski, A., Brovkin, V., Claussen, M., Eliseev, A., Kubatzki, C., and Rahmstorf, S.: CLIMBER-2: a climate system model of intermediate complexity. Part I: model description and performance for present climate, *Clim. Dyn.*, 16, 1–17, <https://doi.org/10.1007/PL00007919>, 2000.
- Royer, D. L.:  $\text{CO}_2$ -forced climate thresholds during the Phanerozoic, *Geochim. Cosmochim. Acta*, 70, 5665–5675, <https://doi.org/10.1016/j.gca.2005.11.031>, 2006.
- Sandberg, C. A., Morrow, J. R., and Ziegler, W.: Late Devonian sea-level changes, catastrophic events, and mass extinctions, in: *Catastrophic events and mass extinctions: impacts and beyond*, edited by Koeberl, C. and MacLeod, K. G., pp. 473–487, *Geol Soc Am S 356*, <https://doi.org/10.1130/0-8137-2356-6.473>, 2002.
- Scotese, C. R.: *Atlas of Devonian Paleogeographic Maps, PALEOMAP Atlas for ArcGIS, Volume 4, The Late Paleozoic, Maps 65-72 (Mollweide Projection)*, PALEOMAP Project, Evanston, IL, 2014.
- Simon, L., Goddérís, Y., Buggisch, W., Strauss, H., and Joachimski, M. M.: Modeling the carbon and sulfur isotope compositions of marine sediments: Climate evolution during the Devonian, *Chem Geol*, 246, 19–38, <https://doi.org/10.1016/j.chemgeo.2007.08.014>, 2007.
- Streel, M., Caputo, M. V., Loboziak, S., and Melo, J. H. G.: Late Frasnian–Famennian climates based on palynomorph analyses and the question of the Late Devonian glaciations, *Earth-Sci Rev*, 52, 121–173, [https://doi.org/10.1016/S0012-8252\(00\)00026-X](https://doi.org/10.1016/S0012-8252(00)00026-X), 2000.
- Tsvetsinskaya, E. A., Schaaf, C. B., Gao, F., Strahler, A. H., Dickinson, R. E., Zeng, X., and Lucht, W.: Relating MODIS-derived surface albedo to soils and rock types over Northern Africa and the Arabian peninsula, *Geophys. Res. Lett.*, 29, 67–1–67–4, <https://doi.org/10.1029/2001GL014096>, 2002.
- van Geldern, R., Joachimski, M., Day, J., Jansen, U., Alvarez, F., Yolkin, E., and Ma, X.-P.: Carbon, oxygen and strontium isotope records of Devonian brachiopod shell calcite, *Palaeogeogr Palaeoclimatol*, 240, 47–67, <https://doi.org/10.1016/j.palaeo.2006.03.045>, 2006.

Clim. Past Discuss., <https://doi.org/10.5194/cp-2018-36>  
Manuscript under review for journal Clim. Past  
Discussion started: 16 April 2018  
© Author(s) 2018. CC BY 4.0 License.



Vennemann, T., Fricke, H., Blake, R., O'Neil, J., and Colman, A.: Oxygen isotope analysis of phosphates: A comparison of techniques for analysis of  $\text{Ag}_3\text{PO}_4$ , *Chem Geol*, 185, 321–336, [https://doi.org/10.1016/S0009-2541\(01\)00413-2](https://doi.org/10.1016/S0009-2541(01)00413-2), 2002.